Ultrasensitive chemiluminescent biosensor for the detection of cholesterol based on synergetic peroxidase-like activity of MoS_2 and graphene quantum dots

Javad Hassanzadeh, Alireza Khataee

www.elsevier.com/locate/talanta

PII: S0039-9140(17)30935-9
DOI: http://dx.doi.org/10.1016/j.talanta.2017.08.107
Reference: TAL17903

To appear in: *Talanta*

Received date: 15 June 2017
Revised date: 7 August 2017
Accepted date: 31 August 2017

Cite this article as: Javad Hassanzadeh and Alireza Khataee, Ultrasensitive chemiluminescent biosensor for the detection of cholesterol based on synergetic peroxidase-like activity of MoS_2 and graphene quantum dots, *Talanta,* http://dx.doi.org/10.1016/j.talanta.2017.08.107

Ultrasensitive chemiluminescent biosensor for the detection of cholesterol based on synergetic peroxidase-like activity of MoS_2 and graphene quantum dots

Javad Hassanzadeh,[a] Alireza Khataee [a,b,*]

[a] Research Laboratory of Advanced Water and Wastewater Treatment Processes, Department of Applied Chemistry, Faculty of Chemistry, University of Tabriz, 51666-16471 Tabriz, Iran

[b] Department of Materials Science and Nanotechnology Engineering, Near East University, 99138 Nicosia, North Cyprus, Mersin 10, Turkey

*Corresponding Author: Tel.: +98 41 33393165; Fax: +98 41 33340191. E–mail: a_khataee@tabrizu.ac.ir

ABSTRACT

Developing a novel non-enzyme mimetic in biosensors is of great significance. Here, a synergetic peroxidase-like activity was disclosed for mixed MoS_2 quantum dots (MoS_2 QDs) and graphene quantum dots (GQDs). The high catalytic effect of this mixture was studied on the chemiluminescence system. It was observed that the simultaneous presence of MoS_2 QDs and GQDs had a powerful enhancing effect on the chemiluminescence (CL) emission of rhodamine B (RB)-H_2O_2 reaction. MoS_2 QDs and GQDs mixture (prepared with a ratio of 3:2) showed a superior catalytic activity when compared to each of the constituents. A linear relationship was acquired between the CL emission intensity and H_2O_2 concentration in the range of 1.5-460 nmol L^{-1}. On the other hand, since the enzymatic oxidation of cholesterol leads to the production of H_2O_2; the offered CL system was examined to detect cholesterol after its oxidation by cholesterol oxidase (ChOx) enzyme. Herein, a further improvement was achieved by MoS_2 nanosheets. The MoS_2 nanosheets increased the performance of ChOx in cholesterol oxidation process. The obtained results confirmed a highly selective and sensitive determination of cholesterol concentration in a linear dynamic range of 0.08-300 µmol L^{-1}, with a detection limit (3S) of 35 nmol L^{-1}. The developed method was successfully applied for the detection of cholesterol level in human serum samples.

Graphical abstract

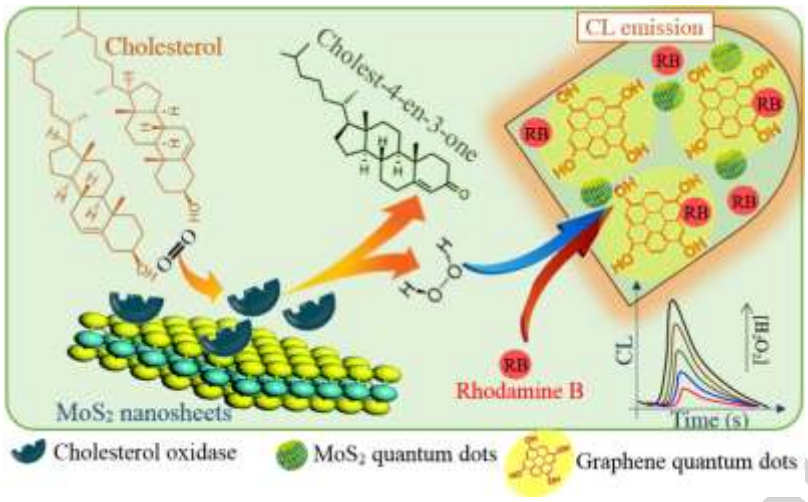

Chemiluminescence sensor for cholesterol using the RB-H_2O_2 CL reaction catalyzed by GQDs/MoS_2 quantum dots.

Keywords: Non-enzyme mimetic; Graphene quantum dots; MoS_2 quantum dots; Cholesterol; Chemiluminescence; Nanosheets.

1. Introduction

Cholesterol (cholest-5-en-3β-ol) and its ester derivatives are one of the necessary structural constituent in the cellular membranes of all animals. Cholesterol provides both the tissue essential integrity and physical versatility. It also has vital roles in brain synapses and immune system. In addition, it is a chief precursor for the formation of steroid hormones, bile acids and vitamin D [1-4]. Higher amounts than normal of cholesterol is termed as hypercholesterolemia, that is the main reason reported for the cardiac arrest hypertension, anemia, coronary heart

disease and other cardiovascular diseases [5, 6]. These disorders are recently counted as the main reasons for human death worldwide. Having a great importance, disciplined and fast assessment of cholesterol of blood has been a universal challenge. The main consideration is on the enzyme based biosensors to convert cholesterol esters to cholesterol form followed by its oxidation using cholesterol oxidase (ChOx). The created H_2O_2 in oxidation process is measured by using various detection techniques, such as electrochemical [7-9], electrochemiluminescence [1, 10], colorimetry [2, 11-14], fluorescence [15, 16], and chemiluminescence (CL) [17, 18] processes. CL method, measuring the light emanated during an oxidation process, is an attractive analytical system owing to its outstanding features. It does not need special skills and can be rapidly carried out using an economic and simple instrumentation. The great sensitivity and very low detection limits are other valuable advantages of CL methods. On the other hand, special nanomaterials have been lately appeared as efficient catalysts in CL systems [19, 20]. In particular, peroxidase nano-mimetics with high catalytic capabilities have introduced wonderful advances in CL-based analysis [17, 18, 21-23]. Several nanomaterials such as metal oxide nanoparticles and various carbon nanostructures [24, 25] with inherent peroxidase-like catalytic activity have been widely applied to identify the biologically important chemicals. The synergistic catalytic effects of a number of nanocomposites such as ZnO/CNT [2], Au NPs/CNT [26] and MoS_2/graphene oxide [27] have been also reported in bio-sensing, with an improved catalytic outcome compered to its constituents.

MoS_2 nanomaterials are attractive artificial peroxidase mimetic with major merits compared to the natural enzymes. The main MoS_2 advantages are: high stability, abundance, low toxicity, simple and cost-effective synthesis, easy storage and suitable optical properties. MoS_2 is comprised of S-Mo-S multilayers with weak van der Waals interactions between the layers [28].

Numerous studies on the catalytic activity of MoS_2 nanostructures has been reported, especially for H_2O_2 detection [27, 29-31]. Li *et al.* [32] investigated the peroxidase-like activity of hemin-capped MoS_2 nanosheets and employed it for the spectrophotometric detection of H_2O_2. Lin and coworkers [29] established a colorimetric biosensor for determination of H_2O_2 and glucose, based on the peroxidase-like activity of MoS_2 nanosheets. Similarly, Xian *et al.* [33] reported peroxidase-like activity of SDS (Sodium dodecyl sulfate) modified MoS_2 NPs as a novel platform for colorimetric detection of H_2O_2 and glucose.

MoS_2 QDs have attracted a considerable attention in recent years [28, 34, 35] for their applications in luminescence-based devices for catalyzing and also bio-imaging purpose [36-40]. To the best of our knowledge, there is no comprehensive report on the synergetic peroxidase-like activity of GQDs and MoS_2 QDs. In the present study, a simultaneous addition of GQDs and MoS_2 QDs to the rhodamine B-H_2O_2 CL system led to a potent enhancement in the CL emission intensity. Based on this effect, a novel and sensitive biosensor was developed for chemiluminometric determination of cholesterol in human blood. After the enzymatic conversion of cholesterol ester derivatives to cholesterol form by cholesterol esterase (ChE), the oxidation of total cholesterol was done in the presence of oxygen by ChOx, which led to the production of H_2O_2. More interestingly, a great improvement in the kinetic factor of enzymatic oxidation of cholesterol was obtained in the presence of MoS_2 nanosheets as an efficient supporting substrate for ChOx. Finally, the produced H_2O_2 in cholesterol oxidation process was added to alkaline rhodamine B solution to generate a chemiluminescence emission in the presence of a mixture of GQDs and MoS_2 QDs as catalyst (Scheme 1). The offered method has outstanding benefits for the cholesterol determination in terms of a simple set-up, great sensitivity and substrate selectivity.

Scheme 1.

2. Experimental

2.1. Apparatus and Materials

CL intensities and profiles were recorded on a Sirius L supersensitive luminometer (Berthold, Germany). Florescence studies were carried out using a LS-45 spectrofluorometer (PerkinElmer, USA). CL spectrum for the mechanism investigation was obtained on the same instrument with a closed excitation slit and in a continuous flow system. UV–visible absorption spectra were achieved by a UV-1800 spectrophotometer (Shimadzu, Japan). Leo 906 (Zeiss, Germany) transmission electron microscope (TEM), Nanosurf Mobile S atomic force microscope (AFM, Swiss) and Mira3 FEG emission scanning electron microscopy (SEM, Czech Republic) were applied for morphology studies of the synthesized nanostructures. The Nanotrac Wave particle size analyser (USA) was used to analyze the size of QDs, based on Dynamic Light Scattering (DLS) phenomenon. X-ray diffraction (XRD) patterns were recorded on a D5000 X-ray diffractometer (Siemens, Germany) by means of Cu Kα exciting source (λ=1.54056 Å). Fourier transform infrared (FTIR) spectra were attained on a Tensor 27 FTIR spectrometer (Bruker, Germany).

All applied chemicals had an analytical grade and applied without further purification. Required solutions were prepared using double deionized (DI) water (Kasra Co. Tabriz, Iran). H_2O_2, glucose, sodium dodecyl sulfate (SDS), N_2H_4, NaOH and RhoB were obtained from Merck (Darmstadt, Germany). MoS_2, Cholesterol, Cholesterol esters, Cholesterol oxidase (100 UN) and Cholesterol esterase (100 UN) were purchased from Sigma. Colorimetric standard kits

for determination of the total cholesterol concentration in serum were from Pars Azmun Co. (Tehran, Iran).

2.2. Synthesis of graphene quantum dots

GQDs were prepared by a simple and rapid method via thermal pyrolysis of glucose powder [41]. Briefly, glucose (6.0 g) was melted on a magnetic hotplate stirrer (IKA RH basic 2, Germany) at 180 °C. The heating was continued for about 2 min, until the color of the colorless melted glucose was changed to dark orange. Then, 25 mL DI water was added and the heat source was removed. The as-prepared GQDs solution was transferred into a dialysis bag (retained molecular weight: 1000 Da) and was floated in deionized water for 32 hours to remove unreacted glucose and other small molecules. The produced GQD solution was sealed and maintained at 4 °C.

2.3. Synthesis of MoS_2 nanosheets and QDs

MoS_2 nanosheets were prepared by a simple exfoliation of MoS_2 powder according a recently reported method [42]. MoS_2 bulk powder was sonicated in a 30% isopropanol/water solvent and in the presence of 4% N_2H_4. The obtained nanosheets was centrifuged (30 min at the speed of 6000 rpm) to collect MoS_2 nanosheets. MoS_2 quantum dots were obtained by thermal treatment of MoS_2 nanosheets. The dispersed MoS_2 nanosheets solution was heated at 120 °C for 4 h and

sonicated for 10 min at 50 °C. The mixture was then centrifuged (2500 rpm, 15 min) to remove the remained MoS_2 nanosheets. The obtained blue solution contained MoS_2 QDs.

2.4. Chemiluminometric detection of H_2O_2 and cholesterol

Cholesterol detection. 100 µL cholesterol standard solution (with different concentrations of cholesterol and cholesterol ester), 100 µL enzyme solution containing of 40 U mL^{-1} ChE and 40 U mL^{-1} ChOx, 50 µL MoS_2 nanosheets solution (25 mg L^{-1}) and 250 µL of 0.01 mol L^{-1} phosphate buffer solution (pH 6.6) were added into an 3 mL Eppendorf tube. The obtained solution was incubated at 37 °C for 5 min until the enzymatic reaction performed and H_2O_2 produced. The obtained solutions were 100-fold diluted using DI water and, a 200 µL was applied to the CL analysis as follows:

H_2O_2 determination. MoS_2 QDs (120 µL), GQDs (80 µL), SDS (2 mmol L^{-1}, 400 µL) and RhoB (2 mmol L^{-1}, 70 µL) solutions together with 80 µL NaOH solution (1 mol L^{-1}) were added into a 3 mL cell, and the final volume of solution was reached to 800 µL by deionized water. 200 µL of H_2O_2 standard solution with different concentrations in the calibration range was injected and the CL intensity was instantaneously followed using luminometer. The maximum intensity was applied as analytical signal. Each analysis was repeated three times.

2.5. Determination of blood cholesterol

In order to detect the cholesterol level in blood, the samples were collected from human volunteers and then were suitably diluted by deionized water. Appropriate amounts of these samples were applied to measure cholesterol according the above mentioned process.

3. Results and discussion

3.1. Characterization of the prepared nanostructures

MoS_2 nanosheets. The SEM image of MoS_2 nanosheets (Fig. 1a) showed a clear layered structure. AFM image were used to further explore the nanosheets morphology (Fig. 1b), which showed the nanosheets with a thicknesses of 3-6 nanometers and sizes in the range of tens to hundreds of nanometers. The TEM image (Fig. 1c) also showed the synthesis of MoS_2 nanostructures with a layered morphology. Moreover, UV-vis absorption spectra were studied to describe the construction of MoS_2 nanosheets (Fig. S1). The diluted dispersion of nanosheets (Inset of Fig. S1) exhibited two specific peaks at about 610 nm and 661 nm that were related to the inherent direct excitonic transitions of MoS_2 with the energy split of the valence band's spin–orbital coupling [29, 43].

MoS_2 QDs. The SEM image of MoS_2 QDs (Fig. 1d) indicated a uniform spherical morphology of the obtained QDs. The destruction of MoS_2 nanosheets after their ultrasonic-modification to QDs was also verified by SEM. The AFM and TEM images of the synthesized solution confirmed the production of spherical QDs (Fig. 1e and 1f) with an average size of about 1.3 nm (inset of Fig. 1e). The DLS results also indicated a narrow size distribution (1-2 nm) for synthesized QDs with an average size of 1.38 (Fig. S2a). As reported previously [43], a

freshly synthesized blue MoS_2 QDs solution (Inset in Fig. S2a) did not show the normal excitonic peaks of MoS_2 (Fig. S2b). Therefore, the absorption spectrum was completely different from nanosheets by a band edge shifted to shorter wavelengths (~330 nm). Quantum confinement in MoS_2 QDs caused a considerable enhancement in the band-to-band transition, and a relatively strong fluorescence emission was observed for the prepared MoS_2 QDs (Fig. 1g). The florescence emission wavelength was dependent on the excitation wavelength, and the maximum emission was obtained at 491 nm with the excitation wavelength of 425 nm (Curve *e* at Fig. 1g). The quantum yield for this emission was calculated 0.8% using RB as reference material.

GQDs. TEM images of the synthesized GQDs revealed the monodisperse nanoparticles with an average diameter of 14.5±4.6 nm (Fig. 2a). HR-TEM image of a single GQD (Fig. 2b) showed an obvious crystal lattice with the lattice parameter of 0.24 nm matching with the (1120) lattice fringe of graphene [44]. Two peaks at about 227 and 278 nm was observed in the specific UV-vis absorption spectra (Fig. 2c) that could be assigned to the $\pi \rightarrow \pi^*$ and $n \rightarrow \pi^*$ vibrations of the aromatic and carbonyl groups, respectively [41]. On the other hand, XRD analysis (Fig. S3a) showed a broad diffraction peak (002) around 18°, indicating the graphite-like structure. The FT-IR spectrum of GQDs (Fig. S3b) showed a number of certain peaks at 1644, 1364 and 2930 cm^{-1} that were attributed to the stretching vibrations of C=O, C=C and C–H bonds, respectively. The broad intense peak at 3359 cm^{-1} and the peak at 1035 cm^{-1} were for the O-H stretching vibrations and C-O bond, respectively. Besides, the excitation dependent fluorescence emission obtained for GQDs [41] are indicated in Fig. 2d. A maximum emission was observed by an excitation wavelength of 360 nm, which provided a great quantum yield of 46% using rhodamine B as reference material.

Fig. 1.

Fig. 2.

All the dispersions of the prepared nanostructures were practically stable at 4 °C for more than 3 months.

3.2. Principle of the chemiluminescence detection system for H_2O_2

H_2O_2 could oxidize RB in basic condition leading to a weak CL emission, which was previously reported in a number of studies [45, 46]. Here, it was observed that the simultaneous presence of GQDs and MoS_2 QDs caused a remarkable intensifying effect on the CL emission at SDS environment (Table S1). The kinetic profiles (Fig. 3a) demonstrated the catalytic effect of each QDs on the RB-H_2O_2 reaction. The emission of RB-H_2O_2 system reached to maximum intensity at about 9 s. However, the maximum CL intensity in the presence of GQDs and MoS_2 QDs mixture was obtained in a shorter time (1 s). This means that the reaction rate is powerfully increased due to the greater catalytic effect of the combined QDs compared with each one alone. On the other hand, no sensible increasing effect was observed for precursor solutions of GQDs and MoS_2 QDs synthesis (Table S1). Accordingly, the discovered catalytic activity was attributed to the existence of GQDs/MoS_2 QDs.

A clear emission spectrum for the developed CL system was obtained (Fig. 3b) with a maximum intensity at λ=578 nm, which is more similar to the fluorescence emission of RB (λ_{em}=575 nm, and λ_{ex}=555 nm). Additionally, a weak emission band was observed at $\lambda\approx$425 nm. The emission intensities in both the wavelengths were proportional to the H_2O_2 concentration.

Thus, it can be preliminarily considered that the oxidation reaction between RB and H_2O_2 generated oxidized RB molecules at electronically excited state (RB_{OX}^*) which could emit at λ≈425 nm [45]. In addition, an efficient energy transfer could be occurred between the RB_{OX}^* species and RB molecules. The produced RB^* more likely acted as emitters and were responsible for CL emission at 578 nm.

Fig. 3.

The catalyzing effect of the applied QDs can be described as follow: the QDs catalyzed the decomposition of H_2O_2 and led to the production of more anion radicals, thus improving the oxidation of RB. The catalyzing ability for MoS_2 QDs was greater than GQDs which was recognized via its higher enhancing effect on CL intensity (Fig. 3a). On the other hand, the fluorescence quenching of RB in the presence of MoS_2 QDs or GQDs (Fig. S4a) demonstrated an efficient interaction between RB molecules and each of the QDs where the RB molecules could be adsorbed on their surfaces. This proximity to QDs could accelerate the energy transfer between RB_{OX}^* and RB species via surface Plasmon process [47]. Furthermore, it can be considered that the electron transferring process from RB to H_2O_2 molecules was facilitated and led to a catalyzed oxidation reaction. This phenomena was confirmed by additional electrochemical tests, as described in the next section.

The synergetic enhancing effect can be also attributed to the electronic interaction between the studied QDs, which was confirmed by emission spectra of GQDs (Fig. S4b). Due to the clear deviation between the Fermi levels of MoS_2 (4.7 eV) and the estimated HUMO level of GQDs (4.2 to 4.4 eV) [48] a partial electron exchange between them was possible [27]. Consequently, the electron-hole pairs were left in GQDs, generating a p-type doped GQDs and suppressing

their fluorescence emission. Conversely, the transferred electrons created a n-type doped MoS_2, leading to charge separation between two types of QDs which could facilitate the oxidation of RB by H_2O_2. The holes in GQD could readily oxidize the RB molecules without any deteriorating effect on the GQD. In contrast, MoS_2 QDs with excess electrons, could interact with H_2O_2 creating more -$OH^{\bullet}$ radicals responsible for the oxidation of RB. The presence of -$OH^{\bullet}$ radicals was also verified using terephthalic acid (TA), as a well-known -$OH^{\bullet}$ probe where the non-fluorescent TA can react with hydroxyl radicals to yield 2-hydroxyterephthalicacid (HTA) with a high fluorescence emission (Fig. 4a). The enhancing effect of the combined GQDs/MoS_2 QDs was relatively higher than each of QDs, wherein a dramatic increase was observed in the fluorescence intensity of TA-H_2O_2 solution. Therefore, the simultaneous existence of both GQDs and MoS_2 QDs could more effectively decompose H_2O_2 to -$OH^{\bullet}$ radicals. The assisting effect of GQDs/MoS_2 QDs was investigated by electrochemical experiments.

3.3. Electrochemical studies

The mechanism of GQDs/MoS_2 QDs action in H_2O_2 reactions was also studied by electrochemical method. A GQDs/MoS_2 QDs-modified glassy carbon electrode (GCE) was prepared and its electrocatalytic activity in the electrochemical reduction of H_2O_2 was followed by cyclic voltammetry and amperometry systems (Fig. 4b). The electrode showed a clear current for H_2O_2 that reached a steady-state value. No obvious current was obtained in the absence of H_2O_2. The outcomes revealed the high efficient electron transferring between electrode and

H_2O_2. Consequently, it can be considered that the GQDs/MoS_2 QDs could assist the electron transfer from RB to H_2O_2 in the oxidation process. The RB molecules on the surface of QDs acted as electron donor and increased their electron density [49, 50]. As a result, the electron transferring process to H_2O_2 would be occurred with a high speed, increasing oxidation rate of RB.

3.4. Peroxidase mimetic properties of GQDs/MoS_2 QDs

To further study on the peroxidase mimetic properties of GQDs/MoS_2 QDs mixture, the studies were applied for a number of peroxidase substrates, including 3,3',5,5'-tetramethylbenzidine (TMB) and 2,2'-azino-bis(3-ethyl-benzothiazoline-6-sulfonic acid) (ABTS). The GQDs/MoS_2 QDs mixture could accelerate the oxidation of all substrates by H_2O_2 to yield a colored compound (Fig. 4c, 4d). For example, the oxidation of TMB created a product with a maximum absorbance at 652 nm (Fig. 4e). In the absence of GQDs/MoS_2 QDs or H_2O_2, no reaction took place that demonstrated the necessity for both of them in the oxidation process, similar to horseradish peroxidase (HRP). High mimetic activity of the GQDs/MoS_2 QDs mixture was studied using steady-state kinetics. On the other words, a set of experiments using the oxidation reaction between TMB-H_2O_2 were performed in the presence of GQDs/MoS_2 QDs mixture at a fixed condition and just the concentration for one reagent (TMB or H_2O_2) was changed (Fig. S5a, S5b). The obtained results were compared with data achieved by the same experiments using HRP as peroxidase (Table 1). The obtained initial reaction rates were applied to the double reciprocal of the Michaelis–Menten equation:

$$1/\upsilon = (Km/Vmax).(1/[S]) + 1/Vmax$$

Where, υ and V_{max} (10^{-8} M s^{-1}) show the initial and maximal reaction rate, respectively, [S] and K_m (mM) are the reagent concentration and Michaelies-Menten constant, respectively. The data were in agreement with Michaelis-Menten equation. K_m and V_{max} were calculated by linear Lineweaver-Burk graphs (Fig. S5). A lower K_m was obtained for MoS_2 QDs/GQDs mixture as the enzyme mimic with both TMB and H_2O_2 (Table 1) that indicated its higher affinity to both of substrates. Accordingly, a very small concentration of the substrate was required to achieve the maximum efficacy. The introduced nano-mimic peroxidase had more powerful efficiency in TMB-H_2O_2 reaction compared with HRP (Table 1). It was also stable in a wide temperature range (10-80 °C) and pH (2-13) with an almost constant catalytic activity (Fig. S6). The sustainability of this type of nano-enzymes with relatively low cost, make them as an appropriate choice in various practical fields.

Fig. 4.

Table 1

3.5. Enzymatic reactions in the presence of MoS_2 nanosheets

Cholesterol oxidase (ChOx), a flavin-adenine-dinucleotide (FAD)-containing flavoenzyme, is an alcohol dehydrogenase that catalyzes the dehydrogenation of hydroxyl group in the cholesterol structure. This creates the corresponding Δ^4-3-ketosteroid and H_2O_2. It was observed that MoS_2 nanosheets interestingly increased the efficiency of H_2O_2 production. The kinetic experiments were done to study the catalytic activity of ChOx with or without MoS_2 nanosheets (Fig. 5). As can be seen, an improvement in the reaction time was observed in the presence of

MoS_2 nanosheets, which could be related to the high surface area of MoS_2 nanosheets as an efficient matrix for the physical adsorption of ChOx. The physical adsorption of ChOx on the surface of MoS_2 nanosheets was studied by FTIR spectra (Fig. 6). After exposing to ChOx for a short time, MoS_2 nanosheets showed clear bands for functional groups of immobilized enzyme. The peaks at about 3382 and 1531 cm^{-1} were related to stretching and bending vibration of $–NH_2$ groups, respectively. Stretching vibrations of C=O in the amide and carboxylic acid groups created peaks at 1617 and 1720 cm^{-1}, respectively.

The immobilization of enzymes on a suitable solid surface can protect them from peripheral impacts and improve their stability and efficiency. It can also increase the half-life and catalytic activity of an enzyme [51]. The effect of MoS_2 nanosheets on the stability of ChOx was investigated (Fig. S7). In the presence of MoS_2 nanosheets, ChOx showed a good strength against the pH and temperature alteration (Fig. S7a, S7b). Moreover, the lifetime of ChOx was improved in the presence of MoS_2 nanosheets (Fig. S7c). The ChOx was incubated in a 2.5 mg L^{-1} MoS_2 nanosheets solution for different durations at 25 °C; the results showed that the enzyme preserved its 78% catalytic activity after 5 day. However, in the absence of MoS_2 nanosheets, the catalytic activity of ChOx was reduced to 13 %. Hence, the higher catalytic activity of ChOx in the presence of MoS_2 nanosheets could be ascribed to the modifications in the ChOx features resulted from its physical adsorption on the surface of nanosheets.

Fig. 5.

Fig. 6.

3.6. Analytical figures of merit

In order to gain the highest sensitivity, the main factors involved in the enzymatic or chemilminometric experiments that could influence the results of the analysis, were optimized (See optimization section and Fig. S8 in *supporting information* file). As given in *supporting information file,* the maximum catalytic activity of ChOx was obtained using 2.5 mg L^{-1} MoS_2 nanosheets and 8 U mL^{-1} ChOx at a phosphate buffer solution (5 mmol L^{-1}, pH 6.6). The sufficient amount for ChOx was less than that of used in the similar reported studies, that could be ascribed to the improving effect of the applied MoS_2 nanosheets on the enzyme efficiency. On the other hand, the highest CL signal was attained by 0.14 mmol L^{-1} RB and 0.08 mol L^{-1} NaOH and, a high catalytic activity was observed for MoS_2 QDs/GQDs mixture with a mass ratio of 1:5. This could be because of the agreement between the bilateral interactions of GQDs with MoS_2 QDs and RB molecules. Large number of MoS_2 QDs could limit the surface area of GQDs for RB molecules and thus, reducing the catalytic activity of GQDs.

Under the optimum condition, the CL emission intensity of the presented system was proportional to the concentration of H_2O_2 (Fig. 7a). A calibration graph was obtained over the concentration range of 1.5-460 nmol L^{-1} under the established optimum condition (Fig. 7b). The limit of detection (LOD) was obtained to be 0.4 nmol L^{-1} for H_2O_2 which was calculated by $3S_b/m$ (S_b shows the standard deviation of signals for repetitive determination of 5 blank solutions, and m is the slope of calibration curve). Moreover, the developed system was examined for determination of cholesterol concentration. As indicated in Fig. 8, the CL intensity was intensified by increasing the cholesterol concentration and a linear calibration graph was obtained using the log of I against the log of C (I and C show the CL intensity and cholesterol concentration in mol L^{-1}, respectively). The linear graph was obtained over the range of 0.08-300

μmol L^{-1} cholesterol with a LOD of 35 nmol L^{-1} (log I = 6.48 + 0.883 log C, (R^2=0.9990)). The analytical features of the offered CL method were compared with a number of previously reported methods (Table S2). As can be seen from Table S2, the presented method has a relatively good sensitivity. Despite of a simple and rapid method for synthesis of nanomaterial, a good detection limit was obtained.

On the other hand, the precision of the developed method was investigated by calculating relative standard deviation (RSD) for the repetitive determination of a certain concentration of cholesterol. The RSD values for the five repetitive determinations of 0.5 and 20 μmol L^{-1} were 3.2 and 4.3%, respectively.

The stability for designed biosensor was investigated by its application in certain intervals after its preparation. The results showed that the biosensor was maintained at 4 °C for at least two week (Fig. S9). It was found suitable for public application of this sensor in medical laboratories.

3.7. Selectivity

A set of experiments were performed to demonstrate the adequate selectivity of the fabricated probe for determination of cholesterol, in a constant concentration (1 μmol L^{-1}) and in the presence of probable interfering species with various concentrations. The tolerance limit of the existing species was set at the maximum concentration that caused an error less than 5% in the response of probe. The data in Fig. S10 indicated that the most of the examined compounds did

not have a considerable interfering effect. On the other hand, the real samples were diluted 500 times which can eliminate the potential effects of the interfering compounds, in which the most of the compounds tested even with 5 mmol L^{-1} concentration showed no interfering effect.

3.8. Analytical application

To investigate the validity of the developed method, it was used for determination of cholesterol in human serum samples using standard addition method (Tables S3 and S4). Certain amounts of cholesterol standard were spiked into the samples before any pretreatment and then evaluated by described procedure. The obtained recoveries were given in Table S3, which disclosed the reliability of the achieved results for the real samples.

The determination of free cholesterol in blood was directly carried out using only ChOx (Table S3). ChOx had a great specificity for free cholesterol, but it could not be able to oxidize cholesterol ester. On the other hand, the total cholesterol was detected using both ChE and ChOx (Table S4). The ChE converted cholesterol ester to free cholesterol and then, ChOx oxidized the total cholesterol. In order to more validate the offered chemiluminometric method for determination of cholesterol, it was applied for the analysis of a standard reference material (SRM 1952a-2) including frozen serum (Table S4). There was a good agreement for cholesterol level between the obtained result (5.79 ±0.09 mmol L^{-1}) and certified value (5.93 ±0.10 mmol L^{-1}) assigned by the National Institute of Standards and Technology (NIST).

4. Conclusions

In the present study, a simple and selective chemiluminescence probe was introduced for determination of cholesterol, based on the synergetic peroxidase activity of MoS_2 QDs and graphene QDs. Each of the employed QDs had an enhancing effect on the CL intensity of H_2O_2-rhodamine B reaction. However, the simultaneous presence of the both QDs promoted the CL emission more effectively. The oxidation reaction between cholesterol-oxygen catalyzed by ChOx in the presence of MoS_2 nanosheets produced H_2O_2, which could react with rhodamine B in the presence of QDs to generate a strong CL emission. It was found that MoS_2 nanosheets accelerated the enzymatic oxidation of cholesterol. The conditions were optimized and a linear range of 0.08–300 μmol L^{-1} was obtained with a detection limit of 35 nmol L^{-1} for cholesterol. Free and total cholesterol content of human serum sample were successfully analyzed by the developed method and gave rise to acceptable results.

Acknowledgment

We thank the University of Tabriz and Near East University for the support provided. We also acknowledge the support of Iran Science Elites Federation.

Appendix A. Supporting information

Supplementary data associated with this article can be found in the online version.

References

[1] M. Zhang, R. Yuan, Y. Chai, S. Chen, H. Zhong, C. Wang, Y. Cheng, A biosensor for cholesterol based on gold nanoparticles-catalyzed luminol electrogenerated chemiluminescence, Biosens. Bioelectron. 32 (2012) 288-292.

[2] A. Hayat, W. Haider, Y. Raza, J.L. Marty, Colorimetric cholesterol sensor based on peroxidase like activity of zinc oxide nanoparticles incorporated carbon nanotubes, Talanta 143 (2015) 157-161.

[3] J. Sun, S. Wang, F. Gao, Covalent Surface Functionalization of Semiconducting Polymer Dots with β-Cyclodextrin for Fluorescent Ratiometric Assay of Cholesterol through Host–Guest Inclusion and FRET, Langmuir 32 (2016) 12725-12731.

[4] M. Chebl, Z. Moussa, M. Peurla, D. Patra, Polyelectrolyte mediated nano hybrid particle as a nano-sensor with outstandingly amplified specificity and sensitivity for enzyme free estimation of cholesterol, Talanta 169 (2017) 104-114.

[5] Q. Sun, S. Fang, Y. Fang, Z. Qian, H. Feng, Fluorometric detection of cholesterol based on β-cyclodextrin functionalized carbon quantum dots via competitive host-guest recognition, Talanta 167 (2017) 513-519.

[6] E. Priyadarshini, K. Rawat, Au@carbon dot nanoconjugates as a dual mode enzyme-free sensing platform for Cholesterol, J. Mater. Chem. B 5 (2017) 5425-5432.

[7] A.N. Sekretaryova, V. Beni, M. Eriksson, A.A. Karyakin, A.P. Turner, M.Y. Vagin, Cholesterol self-powered biosensor, Anal. Chem. 86 (2014) 9540-9547.

[8] A.K. Giri, C. Charan, S.C. Ghosh, V.K. Shahi, A.B. Panda, Phase and composition selective superior cholesterol sensing performance of ZnO@ZnS nano-heterostructure and ZnS nanotubes, Sens. Actuat. B 229 (2016) 14-24.

[9] B.K. Shrestha, R. Ahmad, S. Shrestha, C.H. Park, C.S. Kim, In situ synthesis of cylindrical spongy polypyrrole doped protonated graphitic carbon nitride for cholesterol sensing application, Biosens. Bioelectron. 94 (2017) 686-693.

[10] S. Tang, Q. Zhao, Y. Tu, A sensitive electrochemiluminescent cholesterol biosensor based on Au/hollowed-TiO_2 nano-composite pre-functionalized electrode, Sens. Actuat. B 237 (2016) 416-422.

[11] T. Lin, L. Zhong, H. Chen, Z. Li, Z. Song, L. Guo, F. Fu, A sensitive colorimetric assay for cholesterol based on the peroxidase-like activity of MoS_2 nanosheets, Microchim. Acta 184 (2017) 1233-1237.

[12] Y. Zhang, Y.-N. Wang, X.-T. Sun, L. Chen, Z.-R. Xu, Boron nitride nanosheet/CuS nanocomposites as mimetic peroxidase for sensitive colorimetric detection of cholesterol, Sens. Actuat. B 246 (2017) 118-126.

[13] V. Sharma, S.M. Mobin, Cytocompatible peroxidase mimic CuO: graphene nanosphere composite as colorimetric dual sensor for hydrogen peroxide and cholesterol with its logic gate implementation, Sens. Actuat. B 240 (2017) 338-348.

[14] Y. He, X. Niu, L. Shi, H. Zhao, X. Li, W. Zhang, J. Pan, X. Zhang, Y. Yan, M. Lan, Photometric determination of free cholesterol via cholesterol oxidase and carbon nanotube supported Prussian blue as a peroxidase mimic, Microchim. Acta 184 (2017) 1-9.

[15] T.T. Bui, S.-Y. Park, A carbon dot–hemoglobin complex-based biosensor for cholesterol detection, Green Chem. 18 (2016) 4245-4253.

[16] A.-L. Hu, Y.-H. Liu, H.-H. Deng, G.-L. Hong, A.-L. Liu, X.-H. Lin, X.-H. Xia, W. Chen, Fluorescent hydrogen peroxide sensor based on cupric oxide nanoparticles and its application for glucose and l-lactate detection, Biosens. Bioelectron. 61 (2014) 374-378.

[17] L. Hong, A.-L. Liu, G.-W. Li, W. Chen, X.-H. Lin, Chemiluminescent cholesterol sensor based on peroxidase-like activity of cupric oxide nanoparticles, Biosens. Bioelectron. 43 (2013) 1-5.

[18] S. Xu, Y. Wang, D. Zhou, M. Kuang, D. Fang, W. Yang, S. Wei, L. Ma, A novel chemiluminescence sensor for sensitive detection of cholesterol based on the peroxidase-like activity of copper nanoclusters, Sci. Rep. 6 (2016) doi:10.1038/srep39157.

[19] Y. Su, Y. Xie, X. Hou, Y. Lv, Recent advances in analytical applications of nanomaterials in liquid-phase chemiluminescence, Appl. Spectrosc. Rev. 49 (2014) 201-232.

[20] Y. Su, D. Deng, L. Zhang, H. Song, Y. Lv, Strategies in liquid-phase chemiluminescence and their applications in bioassay, TrAC, Trends Anal. Chem. 82 (2016) 394-411.

[21] W. Chen, L. Hong, A.-L. Liu, J.-Q. Liu, X.-H. Lin, X.-H. Xia, Enhanced chemiluminescence of the luminol-hydrogen peroxide system by colloidal cupric oxide nanoparticles as peroxidase mimic, Talanta 99 (2012) 643-648.

[22] M. Vázquez-González, W.-C. Liao, R.m. Cazelles, S. Wang, X. Yu, V. Gutkin, I. Willner, Mimicking Horseradish Peroxidase Functions Using Cu^{2+}-Modified Carbon Nitride

Nanoparticles or Cu2+-Modified Carbon Dots as Heterogeneous Catalysts, ACS Nano 11 (2017) 3247-3253.

[23] S. Wang, R.m. Cazelles, W.-C. Liao, M. Vázquez-González, A. Zoabi, R. Abu-Reziq, I. Willner, Mimicking Horseradish Peroxidase and NADH Peroxidase by Heterogeneous Cu^{2+}-Modified Graphene Oxide Nanoparticles, Nano Lett. 17 (2017) 2043-2048.

[24] H. Wei, E. Wang, Nanomaterials with enzyme-like characteristics (nanozymes): next-generation artificial enzymes, Chem. Soc. Rev. 42 (2013) 6060-6093.

[25] Y. Lin, J. Ren, X. Qu, Catalytically active nanomaterials: a promising candidate for artificial enzymes, Acc. Chem. Res. 47 (2014) 1097-1105.

[26] X. Cai, X. Gao, L. Wang, Q. Wu, X. Lin, A layer-by-layer assembled and carbon nanotubes/gold nanoparticles-based bienzyme biosensor for cholesterol detection, Sens. Actuat. B 181 (2013) 575-583.

[27] J. Peng, J. Weng, Enhanced peroxidase-like activity of MoS_2/graphene oxide hybrid with light irradiation for glucose detection, Biosens. Bioelectron. 89 (2015) 652-658.

[28] J. Ali, G.U. Siddiqui, K.H. Choi, Y. Jang, K. Lee, Fabrication of blue luminescent MoS_2 quantum dots by wet grinding assisted co-solvent sonication, J. Lumin. 169 (2016) 342-347.

[29] T. Lin, L. Zhong, L. Guo, F. Fu, G. Chen, Seeing diabetes: visual detection of glucose based on the intrinsic peroxidase-like activity of MoS_2 nanosheets, Nanoscale 6 (2014) 11856-11862.

[30] T. Wang, H. Zhu, J. Zhuo, Z. Zhu, P. Papakonstantinou, G. Lubarsky, J. Lin, M. Li, Biosensor based on ultrasmall MoS2 nanoparticles for electrochemical detection of H_2O_2 released by cells at the nanomolar level, Anal. Chem. 85 (2013) 10289-10295.

[31] X. Ou, X. Tan, X. Liu, H. Chen, Y. Fan, S. Chen, S. Wei, A cathodic luminol-based electrochemiluminescence biosensor for detecting cholesterol using 3D-MoS_2–PANI nanoflowers and Ag nanocubes for signal enhancement, RSC Adv. 5 (2015) 66409-66415.

[32] B.L. Li, H.Q. Luo, J.L. Lei, N.B. Li, Hemin-functionalized MoS_2 nanosheets: enhanced peroxidase-like catalytic activity with a steady state in aqueous solution, Rsc Adv. 4 (2014) 24256-24262.

[33] K. Zhao, W. Gu, S. Zheng, C. Zhang, Y. Xian, SDS–MoS_2 nanoparticles as highly-efficient peroxidase mimetics for colorimetric detection of H_2O_2 and glucose, Talanta 141 (2015) 47-52.

[34] N.S. Arul, V. Nithya, Molybdenum disulfide quantum dots: synthesis and applications, RSC Adv. 6 (2016) 65670-65682.

[35] W. Gu, Y. Yan, C. Zhang, C. Ding, Y. Xian, One-Step Synthesis of Water-Soluble MoS2 Quantum Dots via a Hydrothermal Method as a Fluorescent Probe for Hyaluronidase Detection, ACS Appl. Mater. Interfaces 8 (2016) 11272-11279.

[36] Y. Wang, Y. Ni, Molybdenum disulfide quantum dots as a photoluminescence sensing platform for 2, 4, 6-trinitrophenol detection, Anal. Chem. 86 (2014) 7463-7470.

[37] J.Z. Ou, A.F. Chrimes, Y. Wang, S.-y. Tang, M.S. Strano, K. Kalantar-zadeh, Ion-driven photoluminescence modulation of quasi-two-dimensional MoS_2 nanoflakes for applications in biological systems, Nano Lett. 14 (2014) 857-863.

[38] H. Dong, S. Tang, Y. Hao, H. Yu, W. Dai, G. Zhao, Y. Cao, H. Lu, X. Zhang, H. Ju, Fluorescent MoS_2 Quantum Dots: Ultrasonic Preparation, Up-Conversion and Down-Conversion Bioimaging, and Photodynamic Therapy, ACS Appl. Mater. Interfaces 8 (2016) 3107-3114.

[39] Z. Wang, J. Lin, J. Gao, Q. Wang, Two optically active molybdenum disulfide quantum dots as tetracycline sensors, Mater. Chem. Phys. 178 (2016) 82-87.

[40] H.D. Ha, D.J. Han, J.S. Choi, M. Park, T.S. Seo, Dual role of blue luminescent MoS_2 quantum dots in fluorescence resonance energy transfer phenomenon, Small 10 (2014) 3858-3862.

[41] T. Hallaj, M. Amjadi, J.L. Manzoori, R. Shokri, Chemiluminescence reaction of glucose-derived graphene quantum dots with hypochlorite, and its application to the determination of free chlorine, Microchim. Acta 182 (2015) 789-796.

[42] G. Liu, H. Ma, I. Teixeira, Z. Sun, Q. Xia, X. Hong, S.C.E. Tsang, Hydrazine-Assisted Liquid Exfoliation of MoS_2 for Catalytic Hydrodeoxygenation of 4-Methylphenol, Chem. Eur. J. 22 (2016) 2910–2914.

[43] Z. Gan, L. Liu, H. Wu, Y. Hao, Y. Shan, X. Wu, P.K. Chu, Quantum confinement effects across two-dimensional planes in MoS_2 quantum dots, Appl. Phys. Lett. 106 (2015) 233113.

[44] C. Hu, Y. Liu, Y. Yang, J. Cui, Z. Huang, Y. Wang, L. Yang, H. Wang, Y. Xiao, J. Rong, One-step preparation of nitrogen-doped graphene quantum dots from oxidized debris of graphene oxide, J. Mater. Chem. B 1 (2013) 39-42.

[45] J. Abolhasani, M. Amjadi, J. Hassanzadeh, E. Ghorbani-Kalhor, Determination of copper in water by ionic liquid based microextraction and chemiluminescence detection, Anal. Lett. 47 (2014) 1528-1540.

[46] S. Han, E. Liu, H. Li, Flow injection chemiluminescence determination of hemin using the rhodamine B–H_2O_2–NaOH system, Microchim. Acta 149 (2005) 281-286.

[47] J. Hassanzadeh, A. Khataee, N. Bagheri, R. Lotfi, Sensitive chemiluminescence determination method for 2, 4, 6-trinitrotoluene based on the catalytic activity of amine-capped gold nanoparticles, New J. Chem. 41 (2017) 134-141.

[48] Z. Li, R. Ye, R. Feng, Y. Kang, X. Zhu, J.M. Tour, Z. Fang, Graphene quantum dots doping of MoS_2 monolayers, Adv. Mater. 27 (2015) 5235-5240.

[49] W. Shi, Q. Wang, Y. Long, Z. Cheng, S. Chen, H. Zheng, Y. Huang, Carbon nanodots as peroxidase mimetics and their applications to glucose detection, Chem. Commun. 47 (2011) 6695-6697.

[50] J. Mu, Y. Wang, M. Zhao, L. Zhang, Intrinsic peroxidase-like activity and catalase-like activity of Co_3O_4 nanoparticles, Chem. Commun. 48 (2012) 2540-2542.

[51] M. Royvaran, A. Taheri-Kafrani, A.L. Isfahani, S. Mohammadi, Functionalized superparamagnetic graphene oxide nanosheet in enzyme engineering: a highly dispersive, stable and robust biocatalyst, Chem. Eng. J. 288 (2016) 414-422.

[52] Y. Song, K. Qu, C. Zhao, J. Ren, X. Qu, Graphene oxide: intrinsic peroxidase catalytic activity and its application to glucose detection, Adv. Mater. 22 (2010) 2206-2210.

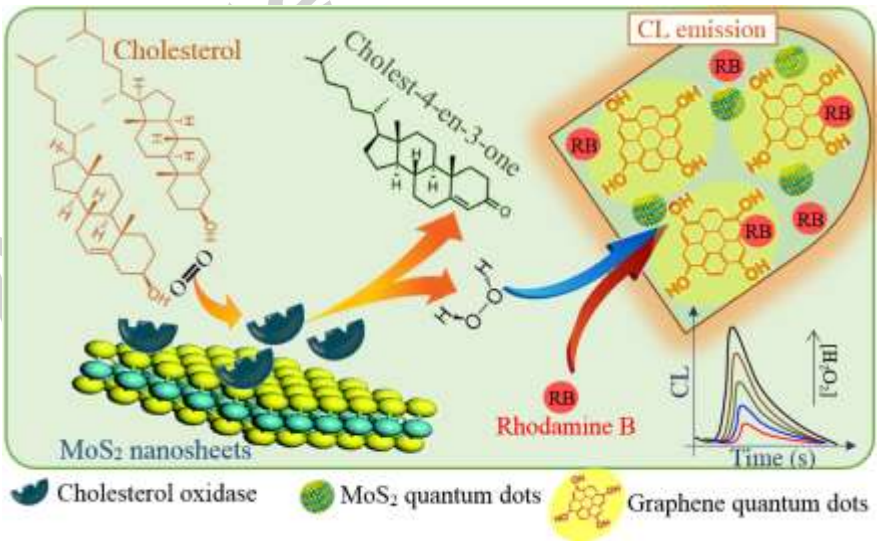

Scheme 1. Schematic illustration of developed chemiluminescence sensor for total cholesterol.

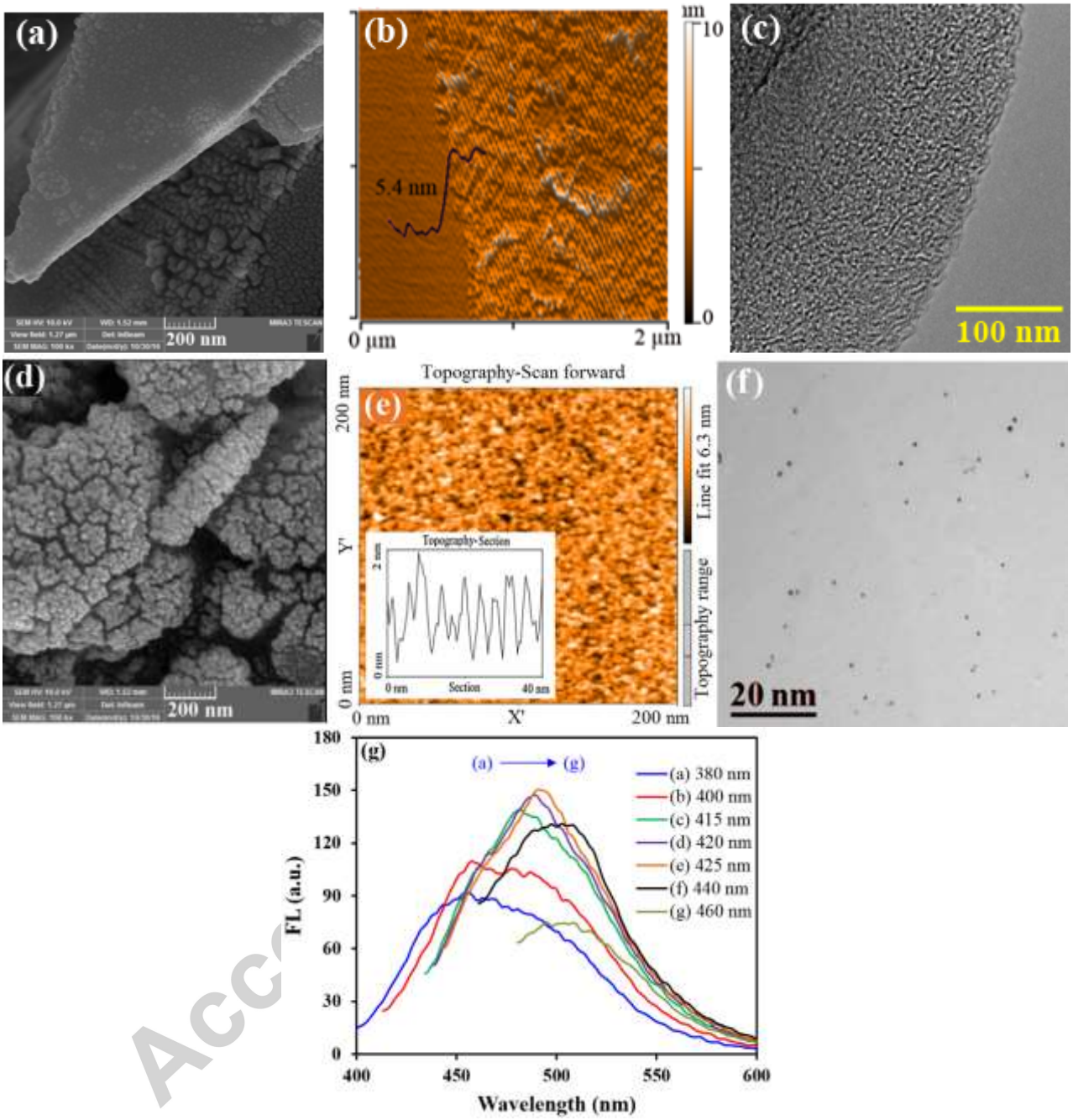
(a)
200 nm
(b)
5.4 nm
nm
10
0
0 µm
2 µm
(c)
100 nm
(d)
200 nm
Topography-Scan forward
(e)
200 nm
Y'
0 nm
Topography-Section
2 nm
0 nm
0 nm
Section
40 nm
0 nm
X'
200 nm
Line fit 6.3 nm
Topography range
(f)
20 nm
(g)
(a) → (g)
(a) 380 nm
(b) 400 nm
(c) 415 nm
(d) 420 nm
(e) 425 nm
(f) 440 nm
(g) 460 nm
FL (a.u.)
180
150
120
90
60
30
0
400
450
500
550
600
Wavelength (nm)

Fig. 1.

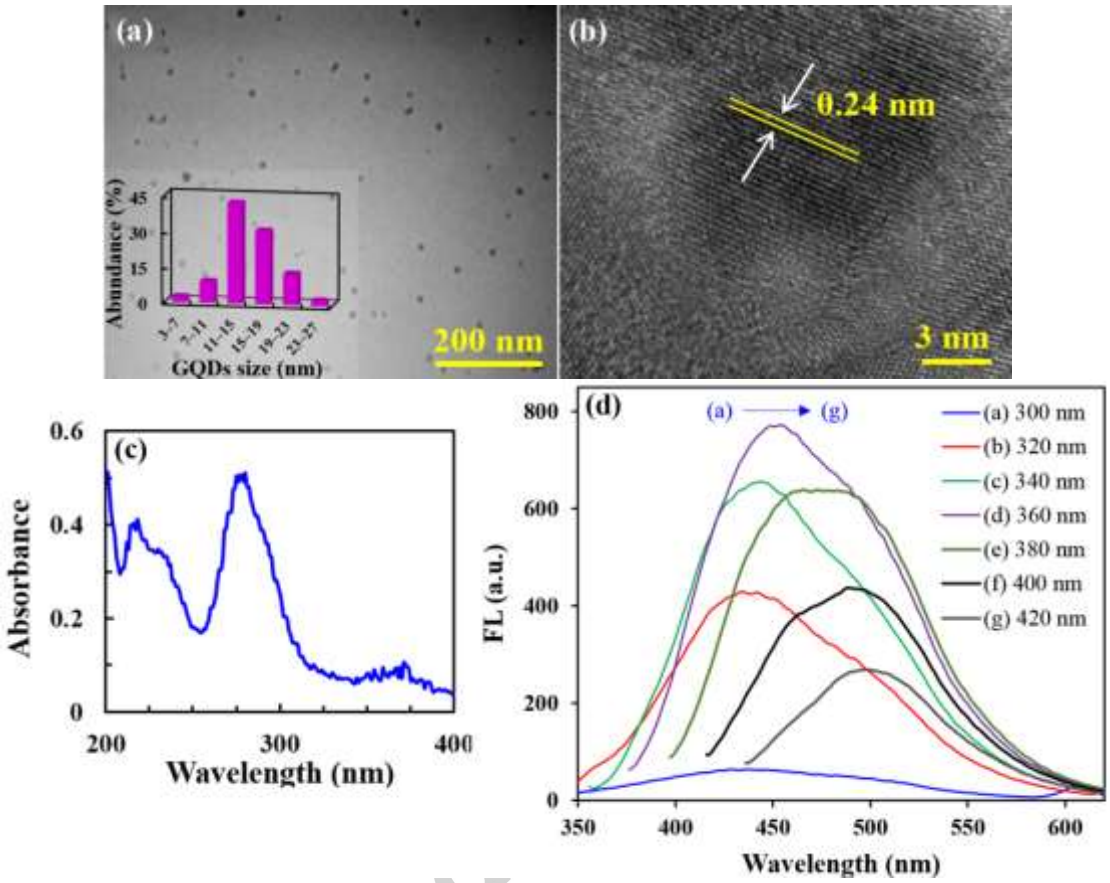

Fig. 2.

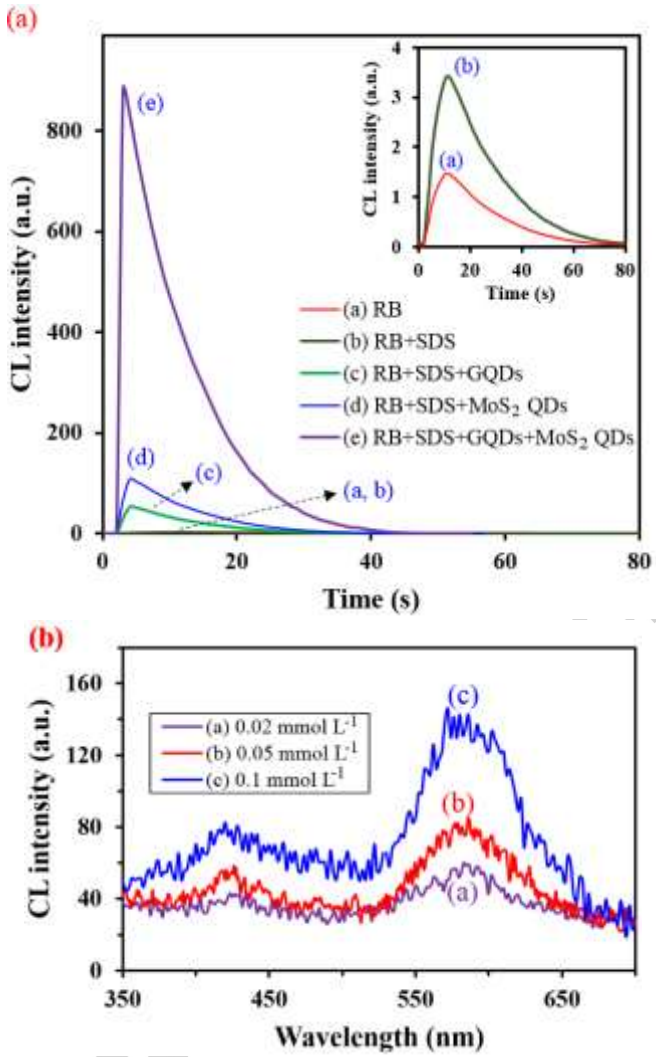
(a)
CL intensity (a.u.)
Time (s)
(e)
(d)
(c)
(a, b)
(a) RB
(b) RB+SDS
(c) RB+SDS+GQDs
(d) RB+SDS+MoS2 QDs
(e) RB+SDS+GQDs+MoS2 QDs
(b)
(a) 0.02 mmol L-1
(b) 0.05 mmol L-1
(c) 0.1 mmol L-1
Wavelength (nm)

Fig. 3.

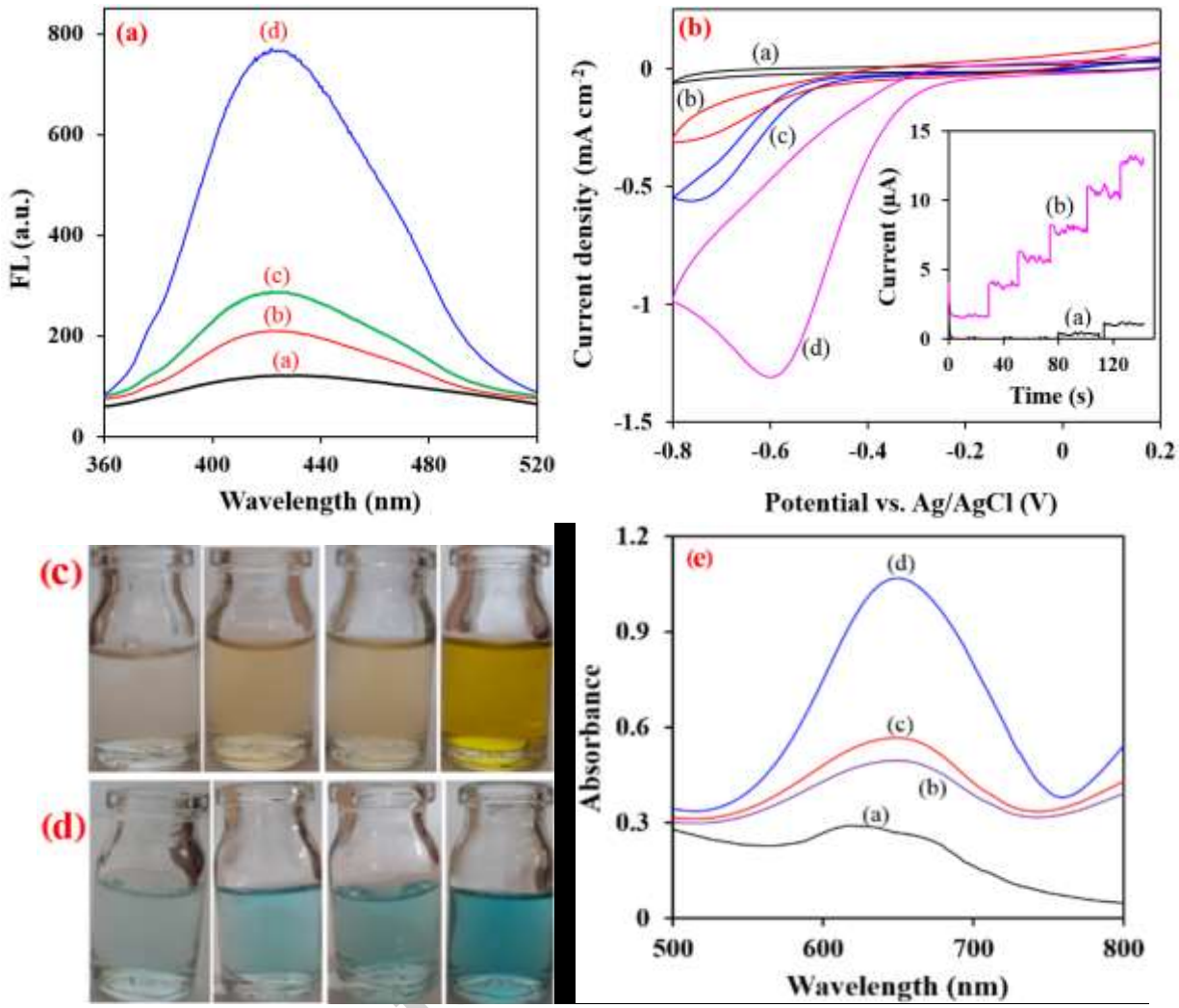

Fig. 4.

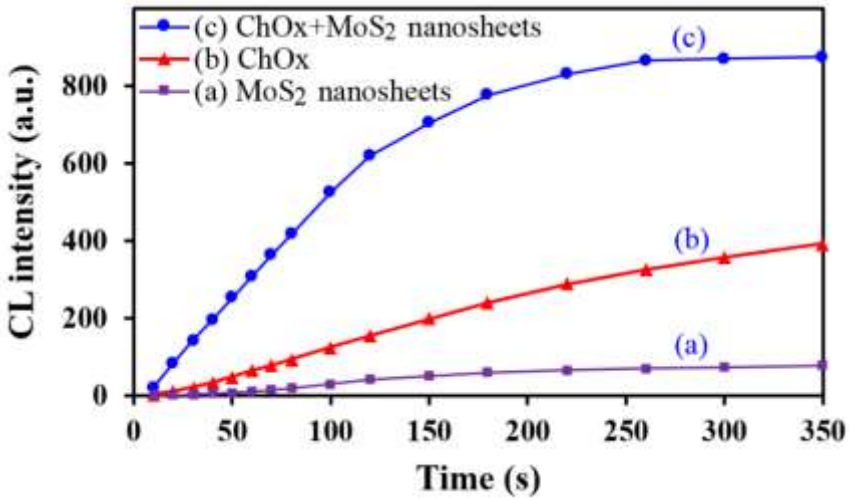

Fig. 5.

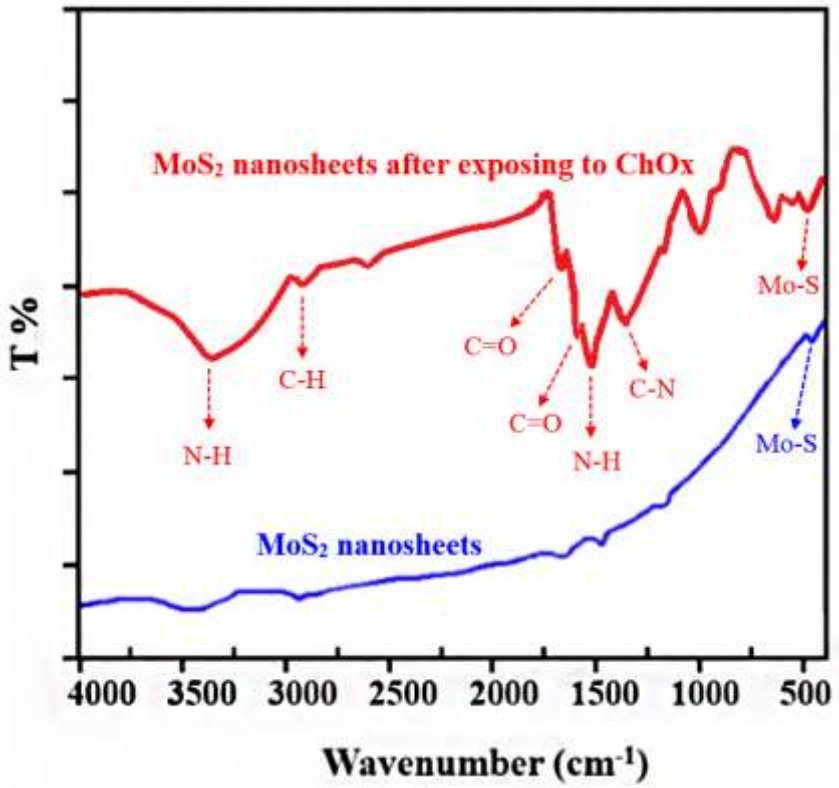

Fig. 6.

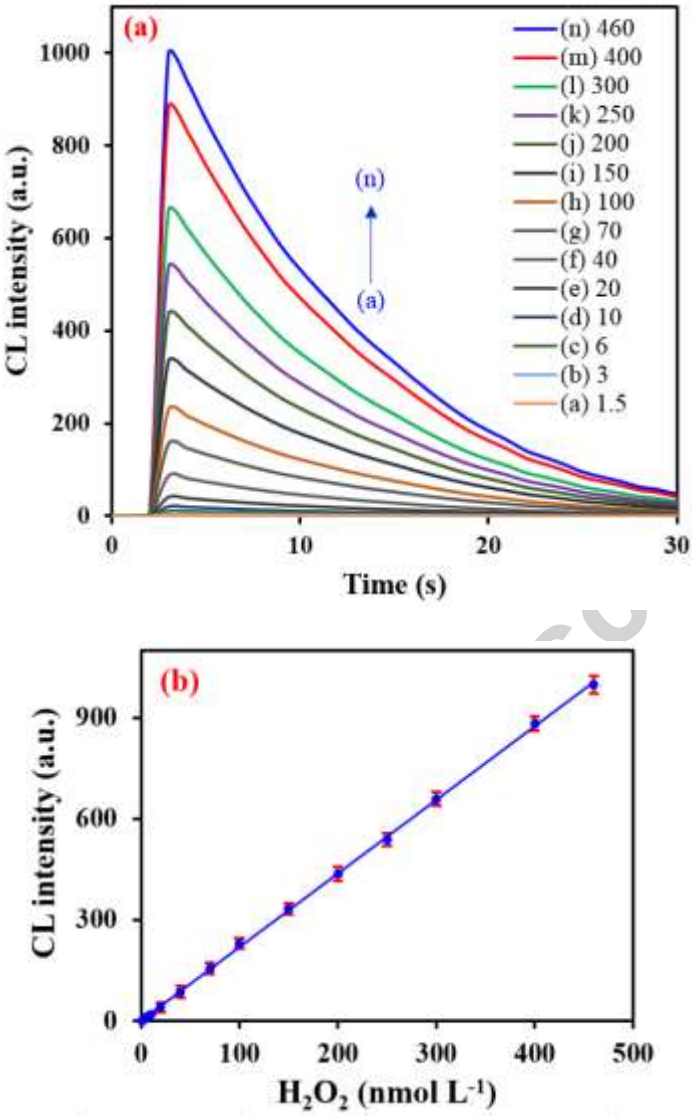
(a)
(n) 460
(m) 400
(l) 300
(k) 250
(j) 200
(i) 150
(h) 100
(g) 70
(f) 40
(e) 20
(d) 10
(c) 6
(b) 3
(a) 1.5
(n)
(a)
CL intensity (a.u.)
Time (s)
(b)
CL intensity (a.u.)
H_2O_2 (nmol L^{-1})

Fig. 7.

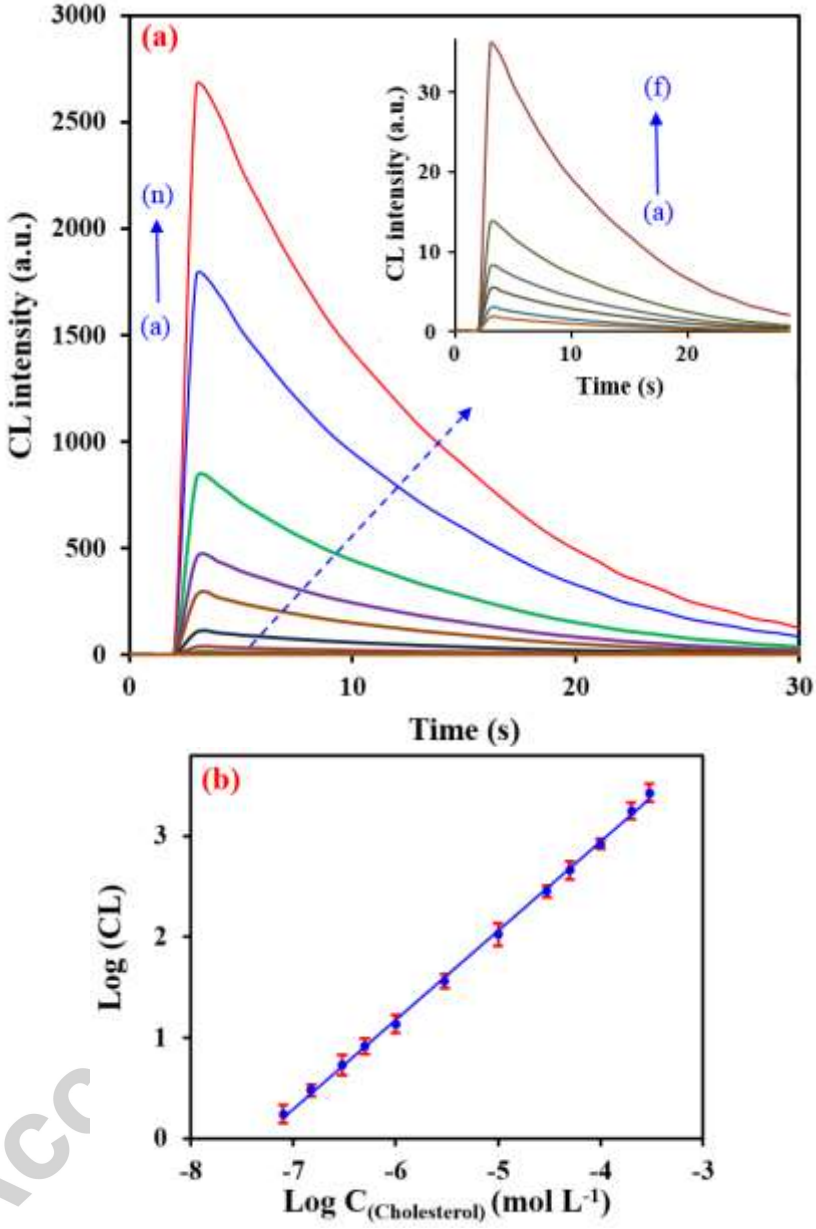
(a)
(n)
(a)
CL intensity (a.u.)
Time (s)
(f)
(a)
CL intensity (a.u.)
Time (s)
(b)
Log (CL)
Log C(Cholesterol) (mol L-1)

Fig. 8.

Figure captions

Fig. 1. SEM (a), AFM (b) and TEM (c) images for synthesized MoS_2 nanosheets; SEM (d), AFM (e) and TEM (f) images for synthesized MoS_2QDs, the inset of *e* shows the height distribution of MoS_2 QDs; (g) fluorescence spectra, with different excitation wavelengths for the synthesized MoS_2 QDs.

Fig. 2. TEM (a) and HRTEM (b) images for synthesized GQDs, the inset of *a* shows the size histogram of GQDs; UV-vis absorption spectrum (c) and fluorescence spectra, with different excitation wavelengths (d) for synthesized GQDs.

Fig. 3. a) Kinetic profiles of different CL systems by addition of 0.01 mmol L^{-1} H_2O_2 [0.14 mmol L^{-1} RB, 0.08 mol L^{-1} NaOH, 0.8 mmol L^{-1} SDS, 0.8 mg L^{-1} GQDs and 1.2 mg L^{-1} MoS_2 QDs]; b) CL spectra for RB-H_2O_2-SDS-GQDs/MoS_2 QDs CL system with different concentrations of H_2O_2 [Obtained in continuous flow state: in one line and 0.5 mmol L^{-1} RB, 0.08 mol L^{-1} NaOH, 1 mmol L^{-1} SDS, 2 mg L^{-1} GQDs and 3 mg L^{-1} MoS_2 QDs in another line].

Fig. 4. a) Fluorescence spectra of TA (0.5mM)-H_2O_2 (10 mM) solution in the absence (a) and presence of GQDs (b), MoS_2 QDs (c) and MoS_2 QDs/GQDs (d). b) Cyclic voltammograms of (a) GCE, (b) MoS_2 QDs-GCE, (c) GQDs-GCE and (d) MoS_2 QDs/GQDs-GCE for the 1 mM H_2O_2 solution [Scan rate: 50 mV s^{-1}]. Inset: amperometric signals of GCE (a) and MoS_2 QDs/GQDs-modified GCE (b) at -0.6 V upon successive additions of 0.5 mM H_2O_2. c, d) Photograph of ABTS (c) and TMB (d) solutions (500 µM) in the presence of 3 mg L^{-1} MoS_2, 2 mg L^{-1} GQDs or their mixture (from left to right) 5 min after injection of 20 mM H_2O_2. e) absorption spectra for TMB (500 µM) in the absence (a) and presence of 3 mg L^{-1} MoS_2 (b), 2 mg L^{-1} GQDs (c), or their mixture (d), 5 min after injection of 20 mM H_2O_2.

Fig. 5. CL intensity-time course curves for H_2O_2 production and the enzymatic oxidation of cholesterol (50 µmol L^{-1}) by ChOx; the rate of oxidation process in the presence of (a) MoS_2 nanosheets (2 mg L^{-1}), (b) ChOx (8 U mL^{-1}) and (c) ChOx (8 U mL^{-1})/MoS_2 nanosheets (2 mg L^{-1}) mixture.

Fig. 6. FTIR spectra for MoS_2 nanosheets before and after their exposing to ChOx solution for 10 min.

Fig. 7. CL profiles of RB-H_2O_2-SDS-MoS_2/GQDs system in the presence of different concentrations of H_2O_2 (nmol L^{-1}) and (b) related calibration graph in optimum condition.

Fig. 8. CL profiles for the determination of cholesterol by RB-H_2O_2-SDS-MoS_2/GQDs CL system in the optimum condition in the presence of different concentrations of cholesterol and (b) related log-log calibration graph.

Table 1 Comparison between the maximum reaction rate (V_m) and Michaelies-Menten constant (K_m) for applied peroxidases.

Catalyst	**K_m (mM)**		**V_m (10^{-8} M s^{-1})**	
	TM	**H_2**	**TM**	**H_2O_2**
MoS_2 QDs	0.12	0.22	1.11	1.26
GQDs	0.22	0.08	1.34	1.23
MoS_2 QDs/GQDs	0.09	0.02	1.52	1.14
HRP [52]	0.27	0.21	1.24	2.46

Research highlights

- An enhanced peroxidase-like action was observed for mixed MoS_2 and graphene QDs.
- The MoS_2/graphene QDs sensitized the rhodamine B-H_2O_2 chemiluminescence system.
- A sensitive non-enzyme chemiluminescence probe is developed for serum cholesterol.
- The produced H_2O_2 by cholesterol oxidation was detected by chemiluminescence route.
- MoS_2 nanosheets improved the performance of cholesterol oxidase.